CHEMICAL ENGINEERING TRANSACTIONS
VOL. 68, 2018
A publication of AIDIC
The Italian Association of Chemical Engineering
Online at www.aidic.it/cet
Guest Editors: Selena Sironi, Laura Capelli

**ISBN** 978-88-95608-65-5; **ISSN** 2283-9216

# Evaluating the Flow Inside of Portable Wind Tunnels for Odour Measurements

Ramon S. Martins[a], Matheus A. Siqueira[a], Izabele V. F. Toniato[a], Kamila F. Cupertino[a], Ademir A. Prata Jr.[b], Neyval C. Reis Jr. [a], Richard M. Stuetz [b], Jane M. Santos[a]*

[a]Department of Environmental Engineering, Universidade Federal do Espírito Santo, Av. Fernando Ferrari, 514, Vitória, ES, Brazil
[b]UNSW Water Research Centre, School of Civil and Environmental Engineering, The University of South Wales, Sydney, NSW, 2052, Australia
jane.santos@pq.cnpq.br

The portable wind tunnel is one of the devices used to estimate the emission rate of odours from area sources. It has been conceived to provide better representation of the atmospheric boundary layer than the other device largely used for this purpose, namely the dynamic flux chamber. Ideally, the flow profile inside the wind tunnel would be close to a fully developed turbulent boundary layer, leading to better predictions of emission rates. However, its aerodynamic performance is still cause of discussion and clearly motivates further investigation. In the present paper, we use computational fluid dynamics to evaluate the flow inside of a portable wind tunnel and to discuss the necessary changes in geometrical configuration to reach the expected behaviour for such a device. The flow inside the main section of the device - where the incoming air comes in contact with the emitting surface – showed to be quite complex and not as well-behaved as expected. We propose and test other configurations for the device, aiming a scenario closer to the atmospheric boundary layer from an aerodynamic perspective. The alternatives considered include changes in the inlet section of the portable wind tunnel and present reasonable improvements for the velocity distribution, suggesting that small geometry modifications can lead to better aerodynamics.

## 1. Introduction

The estimation of odorant gases emission in quiescent area sources, i.e., liquid surfaces with a low degree of disturbance and solid surfaces, such as landfill surfaces and wastewater treatment tanks, presents some difficulties as it is not easy to measure a representative odorant gas concentration and the gas flow is unknown. Therefore, special sampling methods should be adopted to allow the estimation of the emission rate of odorant compounds in these types of sources (Jiang and Kaye, 1996).

The most used method is the direct sampling, using devices that enclosure the gas (Capelli et al., 2012). The principle of direct sampling consists in determining the concentration of the compounds emitted by the sampling surface by enclosing them in a device in which the flow is controlled, and the emission rate is calculated as the product of this concentration and the flow (Jiang et al., 1995). The two main devices used in direct measurements are the dynamic flux chamber and the portable wind tunnel. Studies show that the results obtained with the flux chamber differ from those obtained from the use of the wind tunnel (Hudson and Ayoko, 2009). Based on literature review and theoretical considerations, Hudson and Ayoko (2008) recommend the use of the wind tunnel instead of the flux chamber as odorant compounds can accumulate inside the flux chamber, raising its concentration in the gas phase. This increase in the concentration of the gas can suppress the emission rate of the compound, resulting in an incorrect measurement of the emission rate at the site, differing from the emission that would actually occur in the absence of the flux chamber (Gostelow et al., 2003). Furthermore, the friction velocity on the liquid surface inside the chamber may not match the typical values occurring in the field. The wind tunnel is recommended as an appropriate direct sampling method to evaluate the emission rate of odorant compounds from liquid-gas or solid-gas interface

area sources, especially if this data is used as input for dispersion models, as presented in the work of Capelli et al. (2008) and the reviews by Hudson and Ayoko (2008) and Laor et al. (2014).

Wind tunnels are portable open-bottom compartments that are placed over the emitting surface. In its operation, a part of the emitting surface is isolated and a neutral, odourless air is introduced into the tunnel, simulating the action of the wind on the surface (parallel flow without vertical mixing). The concentration of odour measured at the exit of the tunnel depends on its volatilization from the surface sampled. This phenomenon of mass transfer depends on several factors. While the principal force that determines the emission rate of a compound is the concentration gradient between the two phases (liquid and gas), the magnitude of the Henry's constant ($K_H$) is also very important in determining the mass transfer rate of a compound. The turbulence in the liquid phase is significant for highly volatile materials (with high $K_H$ values), while air turbulence (i.e. wind velocity) is important for the mass transfer velocity in the liquid-gas surface for all compounds, in particular those with small $K_H$ values which is the case for most odorant gases (Hudson and Ayoko, 2008).

There is no universally consensual portable wind tunnel model yet. Variations in the tunnel include differences in the material used in the construction, in the length/width ratio, in the height and in the area of the sampled surface and, consequently, the effect of the flow dynamics on the surface (Smith and Watts, 1994). It is important to take into account that any device used to sample odorant gas disturbs the emitting surface and, therefore, interfere in the emission rate (Hudson and Ayoko, 2008).

The aim of this work consists in analysing the air flow inside the wind tunnel model designed by the University of New South Wales (UNSW) in Australia. The UNSW wind tunnel was aerodynamically designed to create a well-developed boundary layer environment, seeking to simulate a simple atmospheric condition of flow parallel to the emitting surface (Wang et al., 2001). Therefore, numerical simulations were conducted to investigate the influence of different geometry configurations on the flow behaviour.

## 2. Methodology

### 2.1 Tested geometries

The reference case considered is a portable wind tunnel whose dimensions are equal to those of Jiang et al. (1995), and with the outlet extension presented by Wang et al. (2001). The inlet section is formed by a straight pipe section followed by a 180° elbow just upstream of the beginning of the wind tunnel. There is a short transition from a circular to a square cross-section at the very start of the wind tunnel, followed by an expansion section that finishes with the cross-section of the main section. This main section has rectangular cross-section and its bottom is opened in order to provide the mixture between the clean air that enters and the odour compound which is being emitted from the source area. A baffle is installed at the very beginning of the main section aiming to attenuate flow disturbances caused by the upstream curve and expansion. Downstream from the main section, there is a contraction section which facilitates the mixture before the sampling. Finally, a 90° curve starts the outlet extension proposed by Wang et al. (2001) to improve the quality of samples. The geometry of this reference case is shown in Figure 1.

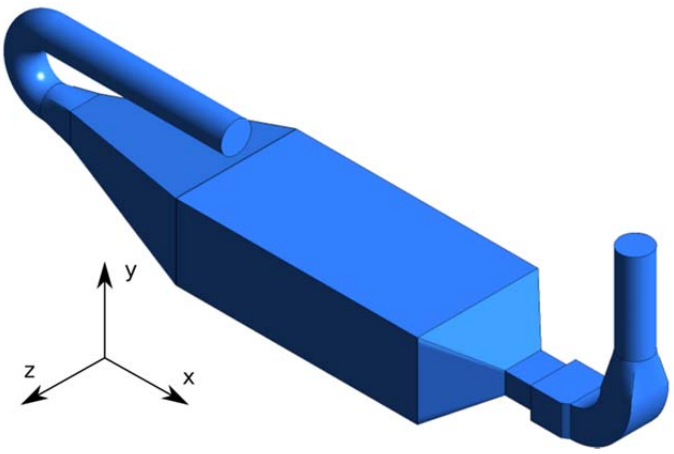


*Figure 1: Schematics of the geometry of the wind tunnel.*

The first alternative to the reference case is shown in Figure 2a, which contains an extended (2 m) straight pipe section at the inlet instead of a curved pipe. This first modification is based on the fact that a curve creates secondary flows, which lead to flow asymmetry and trigger counter-rotating vortexes that increase flow complexity. The second alternative keeps the inlet pipe curved, however a (100 mm long) flow conditioner is added downstream from curve, at the transition section. The main idea here is to diminish the secondary effects caused by the presence of the curve. This configuration is presented in Figure 2b.

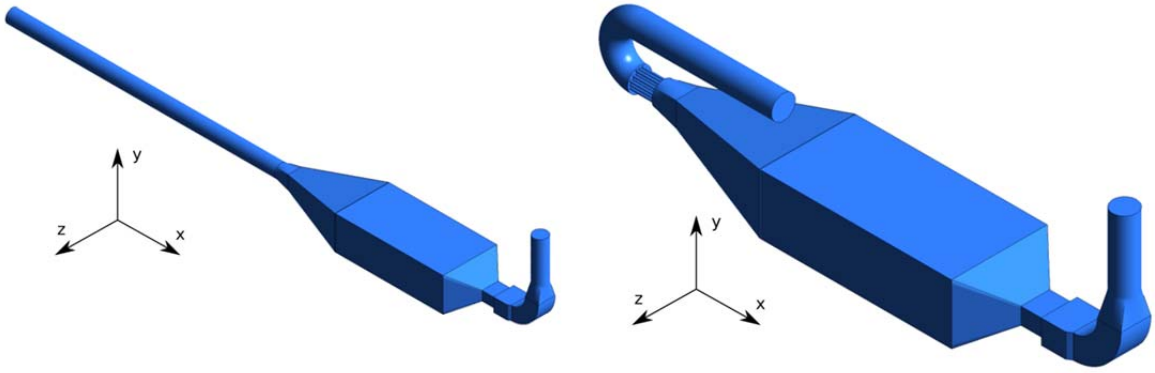


(a) (b)

*Figure 2: Schematics of the modified geometries: (a) extended straight inlet; (b) flow conditioner downstream of the curve.*

### 2.2 Mathematical modelling and numerical methods

The flow of an incompressible Newtonian fluid is modelled by the Navier-Stokes equations. Since the flow inside the portable wind tunnel is turbulent, a Reynolds-Averaged Navier-Stokes (RANS) approach has been chosen to model fluctuating effects. With the adequate statistical treatment, the equations for the balance of mass and momentum get the form

$$\frac{\partial \bar{u}_i}{\partial x_i} = 0 \tag{1}$$

and

$$\bar{u_i}\frac{\partial \bar{u}_j}{\partial x_i} = -\frac{\partial \bar{p}}{\partial x_j} + \frac{\partial}{\partial x_i}\left[(\nu + \nu_T)\left(\frac{\partial \bar{u}_i}{\partial x_j} + \frac{\partial \bar{u}_j}{\partial x_i}\right)\right] \tag{2}$$

Where $u_i$ is the velocity vector, $\rho$ is the density of the fluid, $\nu$ is its kinematic viscosity, $\nu_T$ is the turbulent viscosity, $p$ is the pressure and $x_i$ is the position vector. The turbulent viscosity is obtained by the Shear-stress transport (SST) model with the turbulent kinetic energy ($k$) and the specific dissipation rate ($\omega$) as follows

$$\nu_T = \frac{a_1 k}{max(a_1\omega, DF_2)} \tag{3}$$

The values for $k$ and $\omega$ are obtained from their transport equations, which read

$$\bar{u_i}\frac{\partial k}{\partial x_i} = P_k - \beta_k k\omega + \frac{\partial}{\partial x_i}\left[(\nu + \sigma_k \nu_T)\frac{\partial k}{\partial x_i}\right] \tag{4}$$

and

$$\bar{u_i}\frac{\partial \omega}{\partial x_i} = \alpha D^2 - \beta_\omega \omega^2 + \frac{\partial}{\partial x_i}\left[(\nu + \sigma_\omega \nu_T)\frac{\partial \omega}{\partial x_i}\right] + 2(1 - F_1)\sigma_{\omega 2}\frac{1}{\omega}\frac{\partial k}{\partial x_i}\frac{\partial \omega}{\partial x_i} \tag{5}$$

where, for conciseness, the reader is referred to Menter (1994) for the details concerning the constants and functions of the model.

At the entrance, the uniform velocity of 4.20 m/s is imposed (which provides a mean velocity of 0.33 m/s in the main section, as explored by Jiang et al. (1995)), and the values for $k$ and $\omega$ are estimated as a function of the turbulent intensity and the ratio of the turbulent viscosity to the fluid's viscosity. At the outlet, atmospheric pressure is considered and the derivative of other variables with respect to the normal-to-the-surface direction

is zero. At the wall and at the boundary that represents the air-liquid interface (bottom of the main section) as well, the velocity is null, and the non-slip condition is used. The fluid considered is air, for which $\rho$= 1.225 kg/m$^3$ and $\mu=\nu\rho$= 1.7894 x 10$^{-5}$ Pa s.
The set of equations (1-5) is solved by the commercial CFD software ANSYS Fluent, which is based on the Finite Volume Method. Pressure and velocity are solved in a coupled approach with the "pseudo transient" option, which is a convergence accelerator method. The linear system is solved with the incomplete LU factorization together with the multi-grid method. Gradients are approximated with the cell-based least square scheme, and the convective terms are estimated using the first-order upwind scheme.
All simulations were run until the root mean square of the residual of each equation achieves values smaller than 10$^{-6}$ . with four to eight quad-core machines at 2.8 GHz, 8.0 GB memory and 8 MB cache.

### 2.3 Results

The results for the reference case are now presented. The vertical velocity profiles at the nine different points shown in Fig. 3 are used for comparison. Points number 2, 5 and 8 are aligned with the centreline, points 1, 4 and 7 are on the left side, and points 3, 6 and 9 are on the right side (with respect to the main direction of the flow).

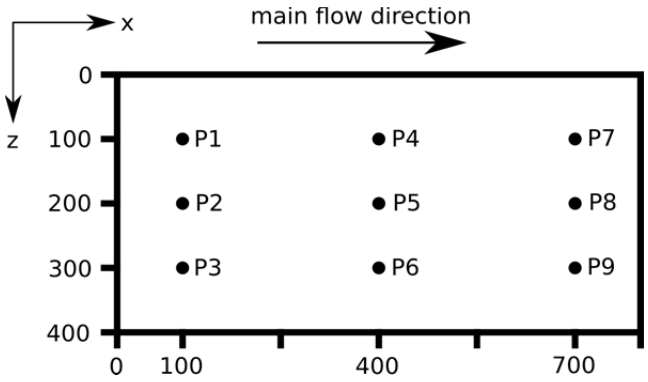


*Figure 3: Sketch representing the location of the points used for the comparisons (lengths in millimetres).*

Figure 4 contains the stream-wise velocity profiles for the reference case at all nine points tested. Each sub-figure gathers the three points distributed in a given stream-wise position (x=100 mm, 400 mm and 700 mm, from left to right).

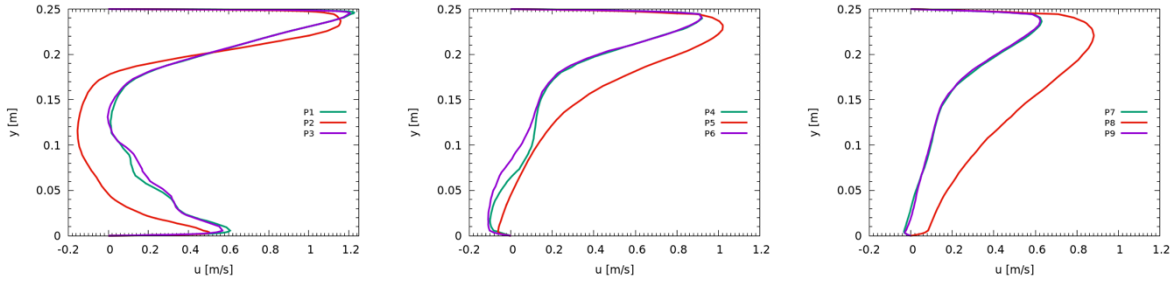


(a) (b) (c)

*Figure 4: Stream-wise velocity profiles at different stream-wise positions: (a) x=100 mm; (b) x=400 mm; (c) x=700 mm.*

Firstly, it is important to remark that the flow profiles at x=100 mm present the highest velocities (around 1.2 m/s) at the top of the main section. The velocities around the half height position are very low. In fact, velocities are even negative at the centre (P2), characterising a backflow condition, and close to zero at the positions close to the sidewalls (P1 and P3)). Approaching to the interface (bottom of the main section), the velocities increase again, reaching maximum values between 0.5 and 0.6 m/s, depending on the span-wise position. Needless to reinforce, because of the no-slip condition, velocity equals zero at the walls and at the interface as well.

At x=400 mm, i.e., at the middle stream-wise line, the velocity profiles are totally shifted towards the top of the wind tunnel. The maximum velocity is about 1 m/s and it rapidly decreases in such a way that the bottom half of the main section presents mainly backflow (negative velocities). This behaviour suggests that the mean flow inside of the main section of the wind tunnel is quite complex, instead of fully-developed or close to an atmospheric boundary layer condition, as ideally thought.

As the flow advances, the velocity profiles clearly tend to equalise. At x=700 mm, there is still a string asymmetry towards the top, but lighter than the one at x=400 mm. In fact, at the centre (P8), the velocities are all positive. Nevertheless, the positions closer to the sidewalls (P7 and P9) still present negative velocities close to the interface.

It is noticeable that the mean flow presents reasonable symmetry with respect to the span-wise direction, regardless of the stream-wise position. This can be observed by comparing the profiles of opposite points (P1-P3, P4-P6 and P7-P9).

Figure 5 shows comparisons between the stream-wise velocity profiles obtained using the modified geometries and the reference case at all nine tested points. The green line (ref) refers to the reference case, the red line (modif 1) is for the extended straight inlet case, and the purple line (modif 2) is for the flow conditioner case.

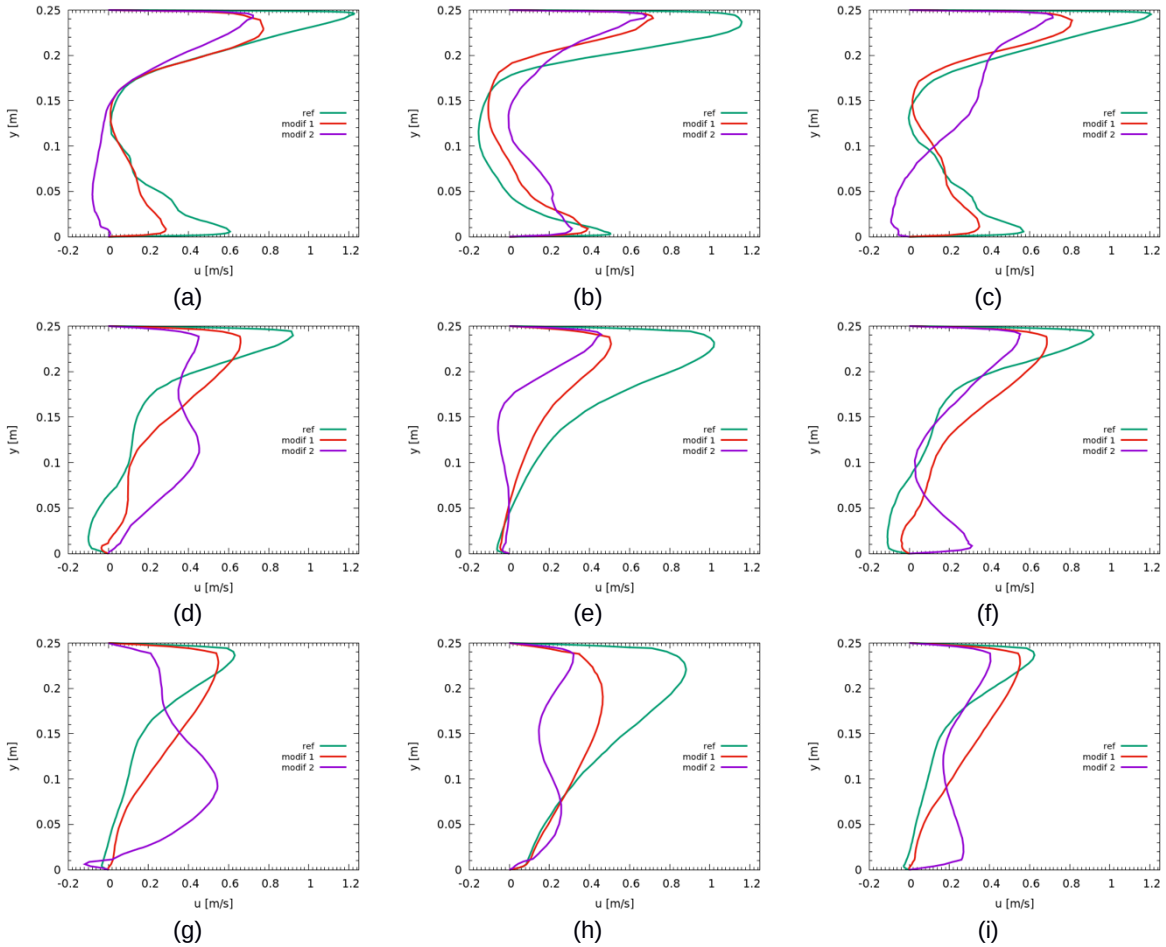


*Figure 5: Comparisons between the velocity profiles obtained for the modified geometries and the reference case at different positions: (a) P1; (b) P2; (c) P3; (d) P4; (e) P5; (f) P6; (g) P7; (h) P8; (I) P9.*

Generally speaking, both modifications led to less deeper velocity gradients, i.e. the velocities tend to be more equally distributed along the vertical direction, therefore, less disturbed. Also, the tendency of the velocity profile to shift towards the top of the main section remains for the modified cases, except for the case with the flow conditioner after the curve at P7, for which the maximum velocity is found in the lower half of the main section.

Replacing the extended straight pipe in place of the curved pipe at the inlet attenuates the differences between maximum and minimum velocities along the vertical direction. At x=100 mm and 700 mm, this

change also strongly diminishes the presence of negative velocities when compared to the reference case. At x=400 mm, some negative velocities are still observed within the lower half of the main section.
The addition of the flow conditioner downstream from the curve led to a significant decrease of the disturbances. However, at some positions, some negative velocities do appear. For instance, at P1 and P3, negative velocities are observed close to the interface, and, at P5, around the half-height. On the other hand, the differences between the upper and lower half of the velocity profile are smaller at x=700 mm when compared to both the reference and the other modified (extended straight inlet) case.

## 3. Conclusions

The velocity profile inside of portable wind tunnels is a crucial issue concerning the estimation of the emission rate of odorant gases. Although there is not a consensual geometry for this device, the design proposed by Jiang et al. (1995) and improved by Wang et al. (2001) is widely used and tested. Numerical simulations of the flow inside this wind tunnel were performed using a commercial CFD code and the velocity profiles obtained inside the main section of the wind tunnel, where the main mass transfer occurs, were analysed.
Some negative velocities appeared close to the interface, which may affect not only the mass transfer but also the accuracy of any model based on fully-developed flow profile or developing boundary layer condition. This fact clearly highlights the motivation of the present paper.
Two modified geometries were proposed, one with an extended straight inlet and the other with a flow conditioner just after the inlet curve. These modifications led to less disturbed profiles (compared to the reference case). In particular, the addition of the flow conditioner after the inlet curve led to the elimination of almost all the negative velocities at the tested positions.
Finally, although small advances were found, there is a clear need for further improvements. An extension of the length of the baffle in the begging of the main section is left as a suggestion to future investigation.

**Acknowledgments**

The authors would like to acknowledge The Brazilian Funding Agency Conselho Nacional de Desenvolvimento Científico e Tecnológico (CNPq) for the financial support to this research through grant number 150413/2017-3.

**References**

Capelli, L. et al., 2008, A comparative and critical evaluation of odour assessment methods on a landfill site, Atmospheric Environment, 42(30), 7050–7058.
Capelli, L. et al., 2012, Validation of a method for odor sampling on solid area sources, Water Science and Technology, 66(8), 1607–1613.
Gostelow, P. et al., 2003, Sampling for the measurement of odours, Scientific and Technical Report, IWA Publishing, 17.
Hudson, N., Ayoko, G., 2008, Odour sampling. 2 - Comparison of physical and aerodynamic characteristics of sampling devices: A review, Bioresource Technology, 99(10), 3993–4007.
Hudson, N., Ayoko, G., 2009, Comparison of emission rate values for odour and odorous chemicals derived from two sampling devices, Atmospheric Environment, 43(20), 3175–3181.
Jiang, K., Bliss, P. J., Schulz, T. J., 1995, The development of a sampling system for determining odor emission rates from areal surfaces: Part 1. Aerodynamic performance, Journal of the Air & Waste Management Association, 45(11), 917–922.
Jiang, K., Kaye, R., 1996, Comparison study on portable wind tunnel system and isolation chamber for determination of VOCs from areal sources. Water Science and Technology, 34(3), 583–589.
Laor, Y.; Parker, D., Pagé, T., 2014, Measurement, prediction, and monitoring of odors in the environment: A critical review. Reviews in Chemical Engineering, 30, 139–166.
Menter, F. R., 1994, Two-equation eddy-viscosity turbulence models for engineering applications, AIAA Journal, 32(8), 1598–1605.
Smith, R.; Watts, P., 1994, Determination of odour emission rates from cattle feedlots: Part 1, A review, Journal of Agricultural Engineering Research, 57(3), 145–155.
Wang, X., Jiang, J., Kaye, R., 2001, Improvement of a wind-tunnel sampling system for odour and VOCs, Water Science and Technology, 44(9), 71–77.